ACS APPLIED MATERIALS & INTERFACES

Research Article

www.acsami.org

Preconditioning of Model Biocarriers by Soluble Pollutants: A QCM-D Study

Hui Huang, Li-li Ding, Hong-qiang Ren,* Jin-ju Geng, Ke Xu, and Yan Zhang

State Key Laboratory of Pollution Control and Resource Reuse, School of the Environment, Nanjing University, Nanjing 210023, Jiangsu, PR China

Supporting Information

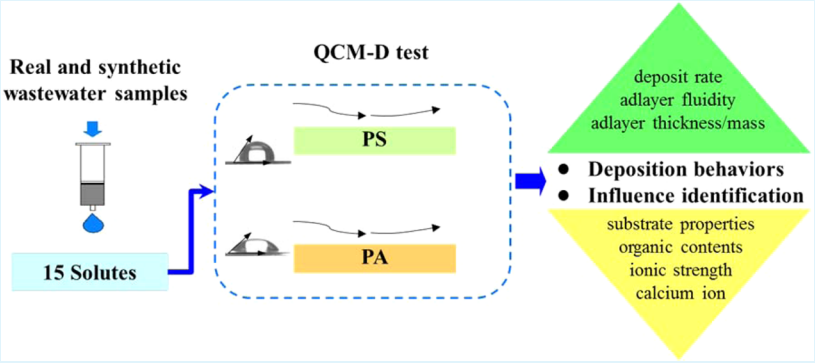

ABSTRACT: Preconditioning of a biocarrier surface is the first step in triggering biofilm formation in attached-growth bioreactors. However, the quantification and control of this step as influenced by solution conditions and biocarrier properties have been rarely explored. In this paper, deposition behaviors of soluble pollutants on the model biocarriers polystyrene (PS) and polyamide (PA) were performed using a quartz crystal microbalance with dissipation monitoring (QCM-D). Three types of wastewater from municipal and industrial wastewater treatment plants and 12 synthetic wastewaters with different configurations of model macromolecules (bovine serum albumin and sodium alginate) and ionic compositions (Na^+ and Ca^{2+}) were prepared. Results showed that high organic contents (protein and humic acid) in real wastewater increased deposition compared to the impact of ions on the two types of carriers. For synthetic wastewater, an interesting phenomenon was observed in that the presence of Ca^{2+} can transform a thin and rigid adlayer into a denser and viscoelastic one on the surface of PS with low organic contents, yet a viscoelastic adlayer can directly form on PS and an increase in the ionic strength hinders deposition in the presence of high organic contents. The deposition of solutes on PA produces a thicker and viscoelastic adlayer that is strengthened an elevated concentration of organic materials. Additionally, a weakening effect of Ca^{2+} on deposition was revealed under high ionic strength. This is the first demonstration of control strategies for preconditioning hydrophilic and hydrophobic biocarriers under different water quality conditions and has important implications for the design of a start-up process for biofilm formation in attached-growth bioreactors.

KEYWORDS: *preconditioning, deposition, biocarrier, soluble pollutants, QCM-D*

1. INTRODUCTION

With improved chemical materials being used as biocarriers, the biofilm process (i.e., the attached-growth process) has been an attractive strategy for upgrading wastewater treatment plants around the world.[1−4] A biofilm in an attached-growth bioreactor is a structured community embedded within a self-produced matrix of extracellular polymeric substance (EPS) and is crucial for the performance of the biofilm process.[5−7] Generally accepted dynamic processes of biofilm formation include (i) preconditioning of the adhesion surface, (ii) adhesion of planktonic cells on the surface and clustering of cells, and (iii) substrate metabolism and EPS production.[7−11] Substratum preconditioning by ambient molecules facilitates bacterial attachment and deposition as the interface interaction may modify the surface characteristics and eventually provide conditions suitable for bacterial retention on the surface.[5,7,12] Therefore, it is important to fundamentally investigate the preconditioning process for a better understanding of biofilm formation. However, the quantification and control methods for preconditioning of biocarriers have been rarely explored.

Compared with very limited experimental methods for substratum preconditioning, such as immersing operation under static conditions[13] and a flowing test based on slides,[14] quartz crystal microbalance with dissipation monitoring (QCM-D) provides a real-time tool for quantifying relatively low levels of deposition (i.e., ng cm^{-2}) and characterizing

Received: January 12, 2015
Accepted: March 18, 2015
Published: March 18, 2015

DOI: 10.1021/acsami.5b00324
ACS Appl. Mater. Interfaces 2015, 7, 7222−7230

biomolecular binding events on the solid−liquid interface.[15,16] It has also recently been proven to be one of the best tools for determining the deposition kinetics of soluble pollutants.[17−20] Soluble pollutants used in QCM-D experiments in previous studies were model macromolecules (e.g., bovine serum albumin (BSA) and sodium alginate (SA)),[12,19,21,22] extracted from pure cultures of bacterial strains,[18,22−24] or based on sewage cultivation under laboratorial conditions,[17,20,25] which might differ considerably from the composition of real wastewater. In addition, ionic composition should be taken into account, as it plays an important role in deposition by affecting polymer−polymer and polymer−substrate interactions at the interface.[18,25−27]

On the other hand, properties of the substrate material also play an important role in preconditioning,[12,13,16,24,28−30] among which surface chemistry (related to wettability and surface charge) and texture (related to specific surface area and roughness) are the two major factors. In previous studies, depositions of BSA and SA on crystal surfaces (polyvinylidene fluoride (PVDF) and SiO_2 account for most cases) under different solution chemistry conditions were investigated through QCM-D experiments.[12,19,21,22] However, depositions of multicomponent solutes having characteristics similar to real wastewater on typical biocarrier surfaces have not to date been fully investigated.

Polystyrene (PS) and polyamide (PA) are representative substrate materials that are used as biocarriers in the biofilm process. They exhibit discrepant characteristics of surface wettabilities. Our previous study has confirmed that a biofilm is easier to form on hydrophilic-engineered biocarriers compared to hydrophobic ones through a 90-day (average) biofilm formation test in three typical full-scale wastewater treatment plants (WWTPs). However, whether the surface wettability-induced difference takes place at the first stage (i.e., the preconditioning stage) of biofilm formation remains to be ascertained.

Therefore, a comparative study on the deposition behavior of soluble pollutants on PS and PA was carried out through QCM-D testing in the present study. Both real wastewater from typical full-scale WWTPs and synthetic wastewater with different configurations of model macromolecules (BSA and SA) and ionic compositions (Na^+ and Ca^{2+}) were prepared as testing solutions. Solute deposition behaviors and influence factors were systematically investigated. To the best of our knowledge, this study is the first attempt at providing new insight into the preconditioning of biocarriers, which may help to obtain clearer information for the design of start-up processes for biofilm formation in attached-growth bioreactors.

2. MATERIALS AND METHODS

2.1. Wastewater Source and Characterization. Real wastewater sourced from aerobic bioreactors in three typical full-scale WWTPs and their descriptions are shown in Table S1 in the Supporting Information (SI). Soluble constituents were obtained from the mixed liquor of wastewater after filtration through a 0.45-μm cellulose acetate membrane (Millipore, USA) within 2 h after sampling and preserved in a refrigerator at ∼4 °C until use.[31] The characteristics of real wastewater were systematically investigated, including pH, conductivity, organic composition indicators composed of total organic carbon (TOC), proteins (PN), polysaccharides (PS), humic acid (HA), metal elements, zeta potential, and fluorescence spectra. The pH value, conductivity, and TOC were measured by standard methods.[32] PN, PS, and HA were determined according to Bradford,[33] DuBois,[34] and Frølund assays,[35] respectively. Metal element contents were measured using inductively coupled plasma-optical emission spectroscopy (ICP-OES, Optima 5300DV, PerkinElmer, USA). Zeta potentials of real wastewater were obtained through a dynamic light scattering particle sizer (ZetaPALS, Brookhaven Instruments, USA). Excitation emission matrix (EEM) fluorescence spectra was performed on a spectrofluorometer (Fluoromax-4, Horiba-JobinYvon, France) according to our previous study.[36] All of the measurements were conducted at ∼25 °C. Triplicate determinations were carried out for pH, conductivity, organic composition indicators, and metal element contents for each sample. Four runs per cycle were chosen for measurement of the zeta potential.

Twelve types of synthetic wastewater samples were prepared according to compositions of real wastewater with three concentration gradients of PN and PS with a constant PN/PS ratio (i.e., 3) and two differentionic strengths (10 and 120 mM) in the presence or absence of 1.5 mM Ca^{2+}, respectively (Table 1).

Table 1. Composition of Synthetic Wastewater

		concentration (mg L^{-1})			
group	subgroup	BSA	SA	ion strength (mM)	ion composition
L1	1	20	20 × 1/3	10	10 NaCl
	2	20	20 × 1/3	10	5.5 NaCl+ 1.5 $CaCl_2$
	3	20	20 × 1/3	120	120 NaCl
	4	20	20 × 1/3	120	115.5 NaCl+ 1.5 $CaCl_2$
L2	1	50	50 × 1/3	10	10 NaCl
	2	50	50 × 1/3	10	5.5 NaCl+ 1.5 $CaCl_2$
	3	50	50 × 1/3	120	120 NaCl
	4	50	50 × 1/3	120	115.5 NaCl+ 1.5 $CaCl_2$
H	1	120	120 × 1/3	10	10 NaCl
	2	120	120 × 1/3	10	5.5 NaCl+ 1.5 $CaCl_2$
	3	120	120 × 1/3	120	120 NaCl
	4	120	120 × 1/3	120	115.5 NaCl+ 1.5 $CaCl_2$

2.2. Source and Characterization of Model Biocarriers. Both the polystyrene (PS, QSX305)- and polyamide (PA, QSX999)-coated crystals were purchased from Q-sense AB (Sweden). Contact angles of double distilled water and real wastewater on the coating surfaces were determined by the sessile drop-tangent method using a drop shape analysis system (DSA100, Krüss, Germany) at room temperature (25 ± 1 °C). At least five measurements at different locations were averaged to obtain the contact angle of each sample.

2.3. QCM-D Experiment and Modeling. Deposition behaviors of real and synthetic wastewater on PS and PA were both investigated in the Q-Sense system (Biolin Scientific AB, Sweden) at 25 °C. Pretreatment of the crystals was referred to Sweity.[17] Likewise, a constant flow rate of 150 μL min^{-1} of fluid in the chamber was applied. The flow schedule was as follows: (i) background solution (i.e., double distilled water); (ii) the tested solution of the wastewater sample; and (iii) background solution. Variations of frequency (f, Hz) and dissipation factor (D) were monitored, and ratios of dissipation factor versus frequency shifts ($\Delta D_n/-\Delta f_n$) were recorded at five overtones (n = 3, 5, 7, 9, and 11). Depending on the average $\Delta D/-\Delta f$ ratios, Sauerbrey and Voigt models were employed to model the adlayer mass and thickness variations, respectively.[30,37−42] The Sauerbrey model is valid for nondissipative to weakly dissipative adlayers with an average $\Delta D/-\Delta f$ ratio smaller than 1×10^{-7} Hz^{-1}

$$\Delta m = C\frac{-\Delta f_n}{n} \quad (1)$$

DOI: 10.1021/acsami.5b00324
ACS Appl. Mater. Interfaces 2015, 7, 7222−7230

Table 2. Properties of Real Wastewater in the Present Study

properties		parameters (sample source)		
		LL (WWTP-1)	HL (WWTP-2)	HH (WWTP-3)
pH		7.66 ± 0.14[a]	7.78 ± 0.16	7.52 ± 0.15
conductivity (μs cm^{-1})		670 ± 13	1992 ± 52	15440 ± 393
organic components (mg L^{-1})	TOC	60.3 ± 2.08	24.6 ± 0.64	197 ± 7.85
	PN	83.2 ± 4.35	16.9 ± 0.72	144 ± 6.14
	PS	33.1 ± 0.95	5.24 ± 0.18	22.4 ± 0.71
	HA	37.4 ± 1.24	8.64 ± 0.26	70.5 ± 2.32
metal element contents (mg L^{-1})	Na	69.6 ± 1.04	297 ± 7.42	2781 ± 305.8
	Ca	50.5 ± 0.61	70.1 ± 0.98	51.2 ± 0.62
	Mg	11.1 ± 0.14	15.9 ± 0.20	10.1 ± 0.12
	K	11.7 ± 0.15	2.99 ± 0.037	22.4 ± 0.27
	P	2.98 ± 0.038	4.97 ± 0.061	6.72 ± 0.082
	Si	3.31 ± 0.041	2.94 ± 0.036	3.97 ± 0.046
	Sr	0.280 ± 0.0096	0.149 ± 0.0053	0.270 ± 0.0096
	Mn	0.082 ± 0.0069	0.028 ± 0.0026	0.184 ± 0.0065
	Ba	0.029 ± 0.0028	0.021 ± 0.0020	0.120 ± 0.0042
	Zn	0.024 ± 0.0026	0.016 ± 0.0014	0.145 ± 0.0053
zeta potential (mV)		−19.6 ± 1.01	−17.0 ± 3.92	−25.5 ± 7.34

[a]One standard deviation.

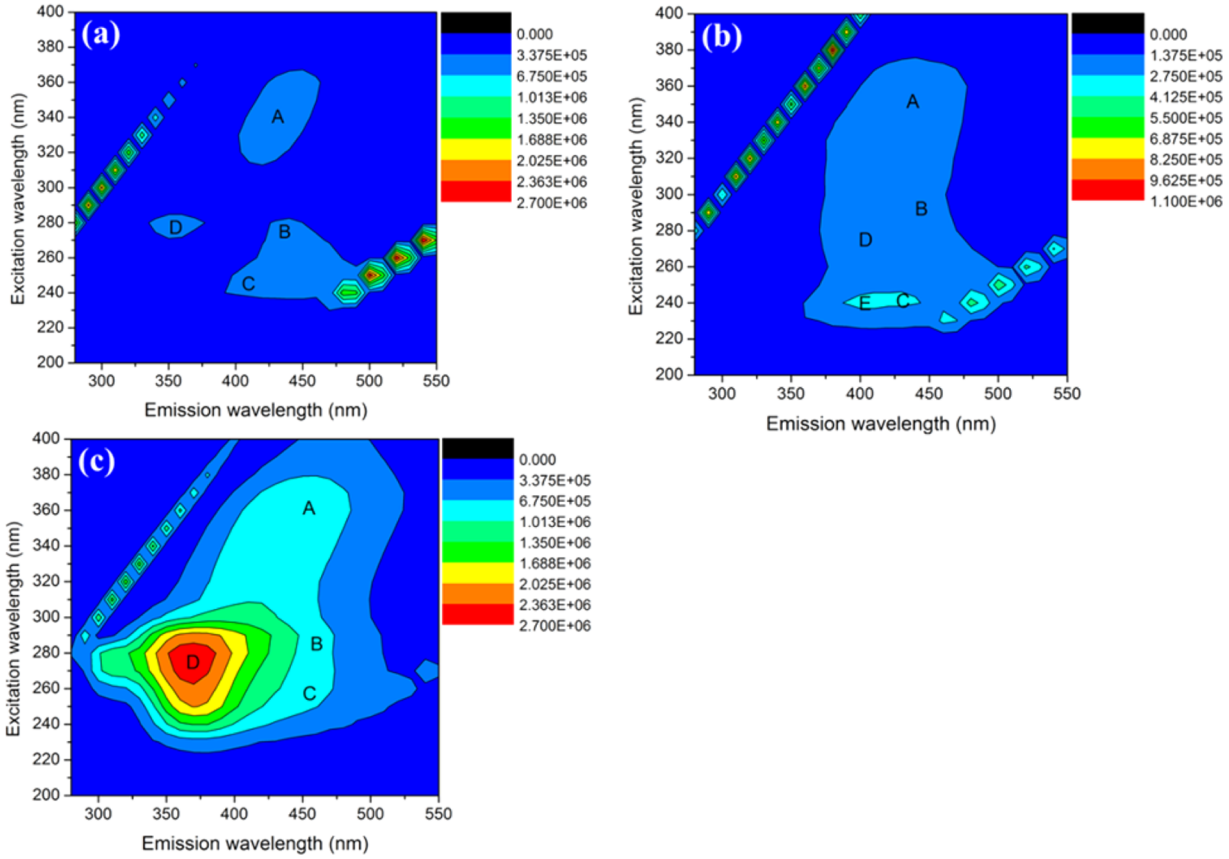

Figure 1. EEM fluorescence spectra of real wastewater with (a) LL, (b) HL, and (c) HH parameters.

where Δm (ng cm^{-2}) is the areal mass density of the adlayer, C (17.7 ng cm^{-2} Hz^{-1}) is the sensor-specific mass sensitivity constant, and Δf_n (Hz) is the frequency shift of the nth overtone. Data from the 3rd overtone were used for calculations and plotting. The Voigt model in the QTool 3 software (Q-Sense) is applied when the average $\Delta D/-\Delta f$ ratio is greater than 1×10^{-7} Hz^{-1}. Data from the 5th, 7th, 9th and 11th overtones were used by this model to calculate the thickness of adlayers under the assumption that adlayers were perfectly homogeneous in density and distribution on the coating surface. The density and viscosity of the fluid and the density of the adlayer were assigned at 1000 kg m^{-3}, 0.001 kg m^{-1} s^{-1}, and 1030 kg m^{-3}, respectively.[17]

Finally, the deposit rate (ng cm^{-2} h^{-1} or nm h^{-1}) was calculated by maximal deposition mass or thickness divided by the duration time, respectively, in which the time span was from the beginning to the time point corresponding to the lowest frequency shift after injection of the tested solutions.

DOI: 10.1021/acsami.5b00324
ACS Appl. Mater. Interfaces 2015, 7, 7222−7230

3. RESULTS AND DISCUSSION

3.1. Characteristics of Real Wastewater. The properties of real wastewater are shown in Table 2. Except for similar neutral pH values, significant differences of chemical parameters were found between the three samples, exhibiting typical water qualities: undoped municipal wastewater with low salinity and low organic concentration (LL), industrial wastewater with high salinity (1095 mg L^{-1} average at 21 ± 1 °C) and low organic concentration (HL), and industrial wastewater with high salinity (8700 mg L^{-1} average at 25 ± 1 °C) and high organic concentration (HH). For the organic indicators, TOC, PN, and HA all exhibited their highest concentrations in HH and lowest concentrations in HL. Na, Ca, and Mg were the main cations in the three samples (other metals not synchronously detected are shown in Table S2 in the SI). The concentration of Na increased in the order LL < HL < HH, whereas the highest concentrations of both Ca and Mg were detected in HL.

Zeta potentials of the three wastewater samples were negative with absolute values <30.0 mV, suggesting instability of the colloidal dispersion. It also became less negative abiding by the order of HH > LL > HL, which was possibly due to divalent ions complexing with biomacromolecules, leading to neutralization of surface charge[22,43−45] because the contents of Ca and Mg ions showed the opposite variations. The variation of in the zeta potential as well as the ion concentrations of the three samples illustrated that compression or shielding effects of the electrostatic double layer by increasing the Ca and Mg ions rather than other cations resulted in a colloid layer with stronger instability and greater electrophoretic mobility.[23,46−48]

Figure 1 showed the EEM fluorescence spectra of the real wastewater samples. Five fluorescence peaks were identified, and their locations and intensities were summarized in Table S3 in the SI. Fluorescence peak E was only found in HL, whereas the other four fluorescence peaks (A, B, C, and D) all emerged in the three samples. Intensities of the four mutual fluorescence peaks also increased following the same orders as those of TOC, PN, and HA as mentioned above, which clearly displayed cross-validation for organic components determined by chemical assays and fluorescence spectroscopy.

All three samples exhibited fluorescence characteristics of a humic acid-like substance (peaks A and B), fulvic acid-like substance (peak C), and soluble microbial product (SMP)-like substance (peak D), which is in accordance with reports from real wastewater samples.[49−51] Additionally, HL showed fluorescence characteristics of an aromatic protein-like substance (peak E), which might be related to the technical process at the fine chemical plant.

3.2. Surface Wettability of PS and PA Coatings. PS and PA coatings exhibited hydrophobic and hydrophilic natures, respectively (images of contact angle determination are shown in Figure S1 in the SI), with water contact angles of 99.8° ± 2.23 and 63.5° ± 1.52, respectively (Table 3). Solute-induced enhancement of wettability was observed as the contact angles of the three real wastewater samples were smaller than those of double distilled water on PS and PA. The contact angles both decreased in the order of LL > HL > HH on two kinds of sensors, implying greater ease of surface wettability enhancement by ions compared to that of organic contents.[43−45] Additionally, little differences were found between contact angles of HL and HH on the same coatings, which will be discussed below.

Table 3. Contact Angles of PS and PA Coatings

	contact angle (deg)	
parameters	PS	PA
water	99.8 ± 2.23[a]	63.5 ± 1.52
LL	98.2 ± 2.14	62.7 ± 1.51
HL	88.9 ± 1.90	54.6 ± 1.36
HH	88.8 ± 1.91	52.3 ± 1.35

[a]One standard deviation ($N \geq 5$).

3.3. Solute Deposition Behavior and Modeling. Normalized frequency and dissipation shifts at the 5th, 7th, 9th, and 11th harmonics (i.e., n = 5, 7, 9, and 11) during the deposition of real wastewater samples were presented as an example in Figure 2 (results using synthetic wastewater are shown in Figures S2−S4 in the SI). A skip point of 30 was applied for the scatterplot. Generally, frequency shifts decreased and dissipation shifts increased at the four overtones along with solution injections with the exception of HL. The frequency shifts first decreased and then increased during injection of HL on PS, implying that desorption of the adlayer occurred due to loose binding force toward the interface. After washing the sensor with water, the frequency increased continuously, which was most likely attributable to the suction of air as the nozzle of the inflow catheter was not immersed in the background solution. The present study has focused on the initial deposition assessment, which was independent of desorption behaviors in the washing stage, and the elapsed time in the first stage (i.e., 194.54 s) was used to calculate the deposit rate of the adlayer on PS.

Dissipation factors versus frequency shifts at the 3th, 5th, 7th, 9th, and 11th overtones during the deposition of all 15 samples tested on the two surfaces are shown in Figure S5 in the SI. Average $\Delta D/-\Delta f$ ratios were calculated and are exhibited in Figure 3a. Taking the value of 0.1×10^{-6} as a threshold, the Voigt and Sauerbrey models were applied for modeling adlayer thickness and mass variations during the deposition, respectively. The Voigt model was suitable for most cases, whereas the Sauerbrey model was only fit for depositions of four tested solutions on PS: L1−3, L2−1, L2−3, and HL. The fitting results of the real wastewater samples as an example are given in Figure S6 in the SI. Finally, the deposit rate (ng cm^{-2} h^{-1} or nm h^{-1}) was calculated and is shown in Figure 3b. Both of the greatest thickness deposit rates (TDRs) of 55.17 nm h^{-1} and 130.19 nm h^{-1} appeared in depositions of HH and L2−2 on PA among real and synthetic wastewater samples, respectively, whereas the mass deposit rate (MDR) had a maximal value of 961.81 ng cm^{-2} h^{-1}, which was found in deposition L2−3 on PS. It is worth mentioning that the $\Delta D/-\Delta f$ ratios were all positive except for two cases, depositions of samples L2−2 and L2−4 on PS (excluded when modeling), which was validated through repeated measurements. This interesting phenomenon implies that such a configuration of the BSA−SA complex and ionic composition may be a turning point for monitoring fluid dynamics on PS, which needs to be further investigated.

3.4. Relationship between Deposit Rates of the Adlayers and Their Fluidities. The $\Delta D/-\Delta f$ ratio represents the magnitude of the variations in the adlayer fluidity, which is the main factor responsible for damping the quartz vibration.[17,52] Thickness and mass deposit rates of the adlayers versus their fluidities during deposition are shown in Figure 4. Negative correlations were observed between the thickness

DOI: 10.1021/acsami.5b00324
ACS Appl. Mater. Interfaces 2015, 7, 7222−7230

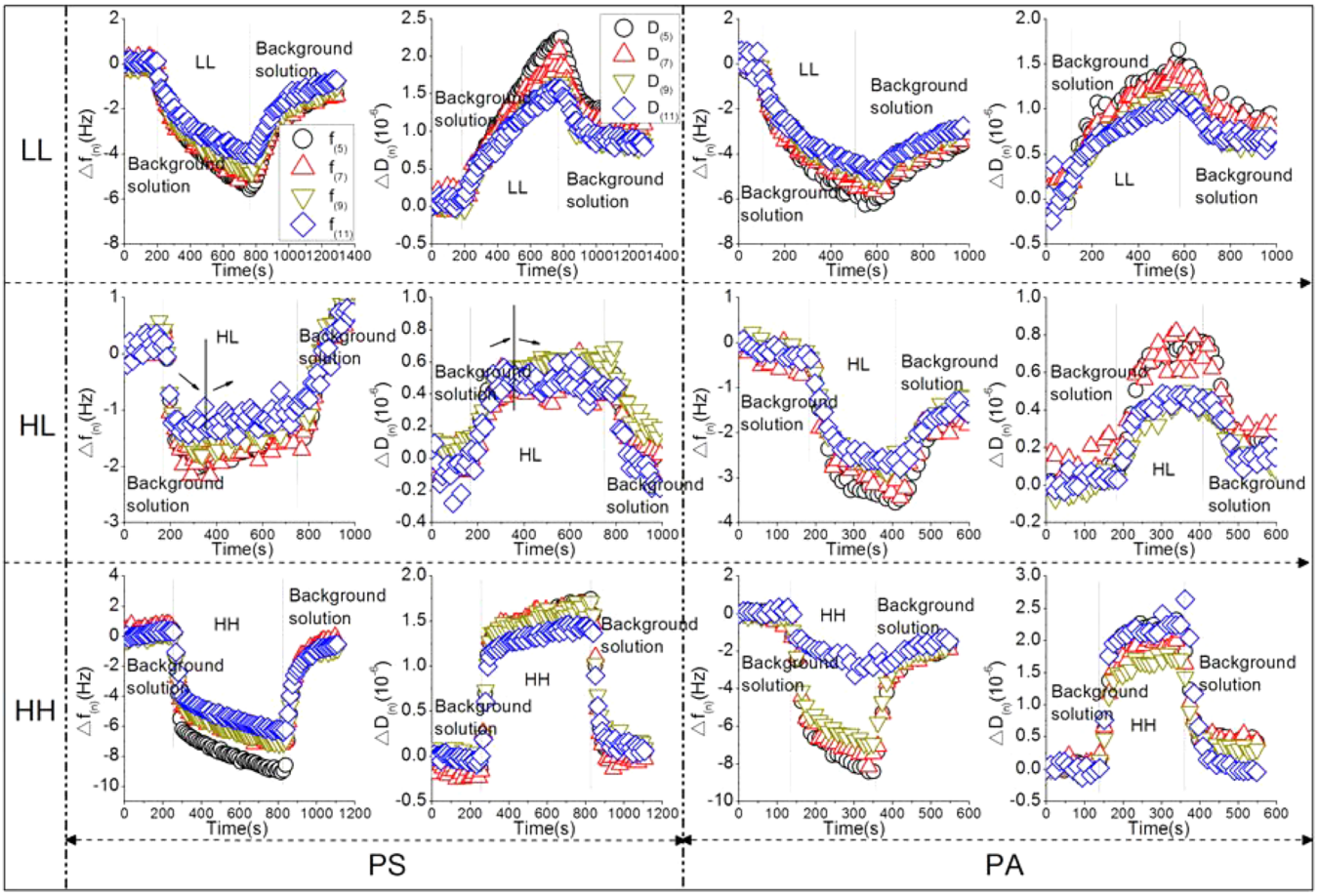

Figure 2. Normalized frequency and dissipation shifts at the 5th, 7th, 9th, and 11th harmonics (i.e., n = 5, 7, 9, and 11) during the deposition of real wastewater on PS and PA surfaces.

deposit rate (TDR) and fluidity in depositions of seven synthetic wastewater samples on PS and those of real wastewater samples on PA, indicating that a more viscoelastic adlayer (corresponding to a higher fluidity) would associate with less thickness. No clear correlation was found between the two parameters when all 12 synthetic wastewater samples were deposited on PA (Figure 4b). Interestingly, the mass deposit rate (MDR) of the adlayer correlated positively with its fluidity on PS (Figure 4a), implying that a more rigid adlayer (corresponding to a smaller fluidity) would result in less mass retention.

3.5. Influence of the Properties of the Substrate Material. PS and PA are representative biocarrier materials that exhibit discrepant characteristics. A clear comparison can be made from Figure 3(b) in that the thickness deposit rates (TDRs) of the tested samples on PA were all greater than those on PS for the same sample with the exception of three cases (L1−2, L1−4 and H-2). The hydrophobic surface inhibits adherence of soluble pollutants to the surface, whereas the hydrophilic surface improves wettability and enhances soluble pollutant deposition. On the other hand, the functional groups in solutes, such as hydroxyl, carbonyl, amino, phenolic hydroxy, and methoxy groups,[46,53] might form hydrogen bonds with acylamino on the surface of PA. Likewise, hydrophobic groups, such as nonpolar groups in solutes, may facilitate the bonding approaching the surface of PS. Subsequent conformational changes may occur, allowing other functional groups to come close enough to the surface to finally result in short-range attractive polymeric interactions.[22,27,54] This may also partially explain the different deposition rates of HL and HH on the same surface despite the similarity in their contact angles.

3.6. Effect of Soluble Components and Surface Charge Characteristic. In the present study, different solution chemistry conditions were designed to reveal the influence of soluble components on deposition behavior. As shown in Figure 3b, thickness deposit rates (TDRs) of the adlayers on PS exhibited distinguishing features among the different groups. Under a low concentration BSA−SA complex (i.e., L1 group), the TDR of the adlayer increased along with increasing ionic strength and Ca^{2+}, whereas under a high concentration of the complex (i.e., H group), it decreased with increasing ionic strength and Ca^{2+}. In addition, the TDRs of the adlayers of real wastewater samples on PS were smaller than those of synthetic wastewater and had similar characteristics, as described under the high concentration of the complex (the TDR of LL was a little higher than that of HH), which was mainly due to interactions between the macromolecules and ions.[44,45,47] Generally, high organic composition enhanced the TDRs of the adlayers on PA in both synthetic wastewater (relatively smaller TDRs in L1 groups) and real wastewater (HH > LL > HL). High ionic strength seemed to facilitate depositions under low organic compositions (L1 group), whereas it had a weakening effect under elevated organic compositions (L2 and H groups). The impact of Ca^{2+} correlated with ionic strength, strengthening and weakening the effects at low and high ionic strength, respectively. It can be

DOI: 10.1021/acsami.5b00324
ACS Appl. Mater. Interfaces 2015, 7, 7222−7230

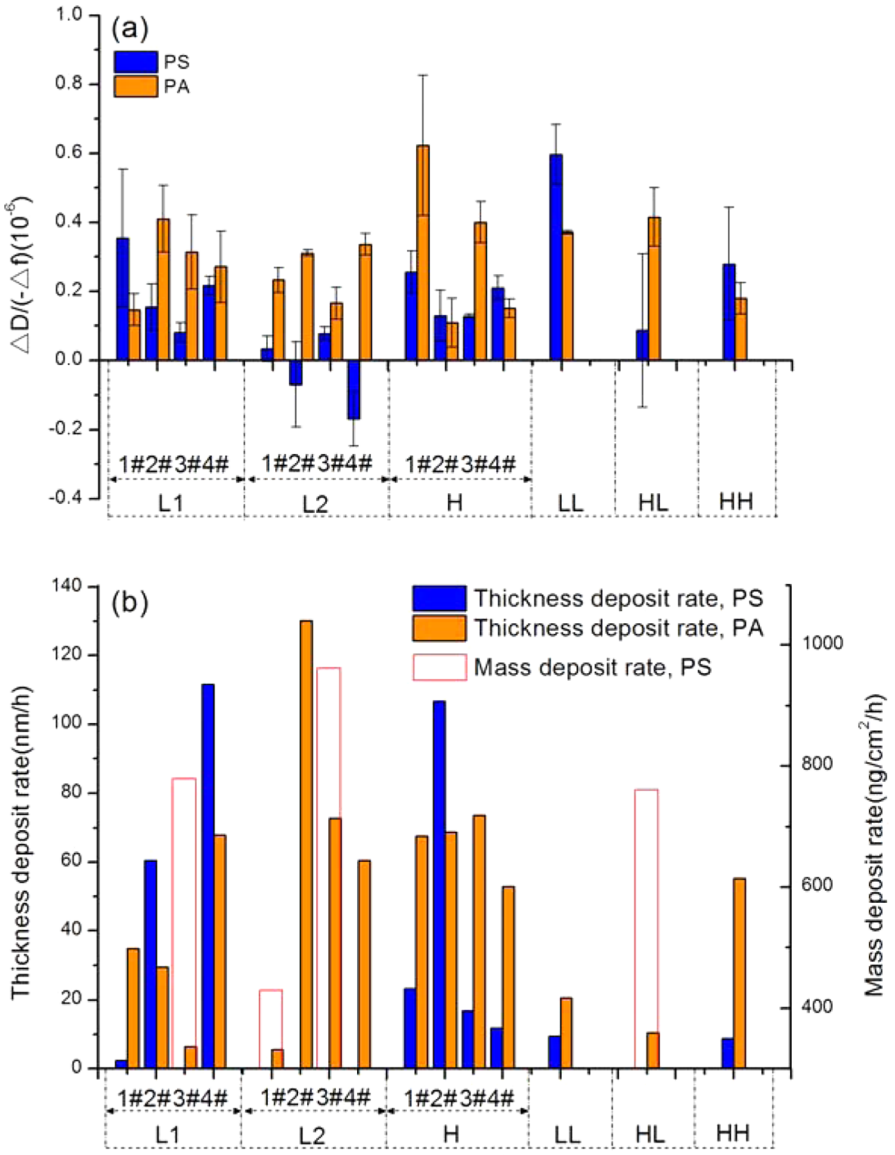

Figure 3. (a) $\Delta D/-\Delta f$ ratios and (b) thickness and mass deposit rates of the adlayers by the Voigt and Sauerbrey models of the tested samples on PS and PA surfaces.

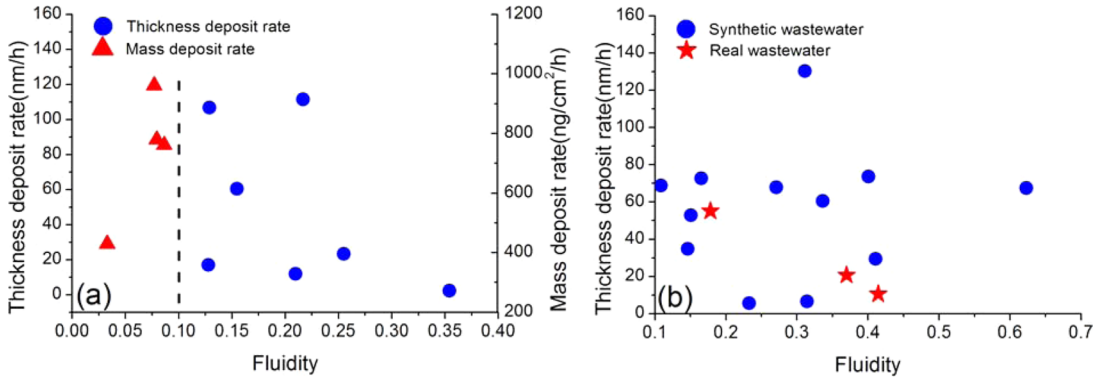

Figure 4. Thickness and mass deposit rates of the adlayers versus their fluidities during deposition on (a) PS and (b) PA.

inferred that the influence of organic concentration is greater than that of ionic strength and Ca^{2+}. This is partially inconsistent with reports that ionic strength (or Ca^{2+}) increases the thickness of the adlayer in multiple studies[18,21,22,25] based on distinguishing configurations of multicomponent systems. As for the mass deposit rate (MDR) of the adlayer on PS, high ionic strength and organic concentration promoted mass deposition (L2−3 > L1−3 > HL > L2−1). MDR was based

DOI: 10.1021/acsami.5b00324
ACS Appl. Mater. Interfaces 2015, 7, 7222−7230

on the Sauerbrey model, and as Ca^{2+} was absent in the three groups of synthetic wastewater listed above, it can be speculated that the presence of calcium helps to promote the formation of viscoelastic films on the surface of PS.

A lower zeta potential (smaller absolute value) implies stronger obstruction of the deposition of real wastewater solutes on PA (TDR: HL < LL < HH). However, the influence of zeta potential on depositions of synthetic wastewater was inconsistent, depending on ionic strength and organic concentration (Figure 3b). These observations are not compatible with the results from some studies[22,46,55] and cannot be explained simply by the classic Derjaguin−Landau−Verwey−Overbeek (DLVO) theory, indicating that deposition is not only governed by electrostatic double layer repulsion but also by non-DLVO processes, such as H-bond forces and electrosteric interactions as discussed above.

3.7. Mechanism of Solute Retention on PS and PA Surfaces. Owing to the short-range attractive polymeric interactions initiated by hydrophobic groups,[22,26,27] solutes in wastewater anchor along the surface of PS to form a thin, rigid film. The addition of calcium enhances solute retention at low ionic strength and organic concentration due to polymer bridging and screening of lateral repulsions between adsorbed polymer molecules, resulting in a thicker and more viscoelastic film. At high ionic strength and organic concentration, the effects of electric double layer compression, screening chain-substrate interactions, and competition of ions for adsorption sites reduce the remaining thickness on the surface to develop a denser adlayer. Hydrophilic interactions, H-bond forces, and electrosteric interactions trigger solutes to stay on the surface of PA[27,46,53−55] and produce a thick, viscoelastic film with high elastic creep of cross-linked biopolymers. A high organic composition leads to a high level of extended conformation and swelling to thicken the adlayer on the surface.[17,20,25] The presence of Ca^{2+} provides a bridge between negatively charged biopolymers and improves the extension of colloidal clusters toward the outside at low ionic strength. Compressed electric double layer and weakened adhesion toward the interface due to possible destabilization of colloidal clusters at elevated ionic strength generally reduce the thickness of the adlayer on the surface of PA.

4. CONCLUSION

In the context of upgrading wastewater treatment plants around the world, this study is the first to demonstrate quantification and control methods for preconditioning model biocarriers under different water quality conditions and has important implications for the design of start-up processes for biofilm formation in attached-growth bioreactors. Our results show that high organic contents in real wastewater on PS and PA increase solute deposition compared to the impact of ions. For synthetic wastewater, the presence of Ca^{2+} can transform a thin, rigid adlayer into a denser, viscoelastic one on the surface of PS under low organic contents; however, a viscoelastic adlayer can directly form on PS and increase in ionic strength to hinder deposition in the presence of high organic contents. The deposition of solutes on PA produces a thicker, viscoelastic adlayer and can be strengthened under an elevated organic concentration. Additionally, a weakening effect of Ca^{2+} on deposition was revealed under high ionic strength. The results also reveal that the deposition of soluble pollutants is governed not only by DLVO interactions but also by non-DLVO processes.

ASSOCIATED CONTENT

Supporting Information

Description of wastewater treatment plants (WWTPs), other metals not synchronously detected in the three real wastewater tests, fluorescence spectral identification of real wastewater, images of contact angle determination, normalized frequency and dissipation shifts during the deposition of synthetic wastewater on PS and PA surfaces, dissipation factors versus frequency shifts during the deposition of tested samples, fitting results of adlayer thickness, and mass variations during deposition. This material is available free of charge via the Internet at http://pubs.acs.org.

AUTHOR INFORMATION

Corresponding Author

*School of the Environment, Nanjing University, N.O. 163, Xianlin Avenue, Qixia District, Nanjing 210023, Jiangsu, PR China. Phone: +86 25 89680512. Fax: +86 25 89680569. E-mail: hqren@nju.edu.cn.

Notes

The authors declare no competing financial interest.

ACKNOWLEDGMENTS

This research was funded by the National High Technology Research and Development Program (863 Program, 2012AA063407), the Natural Science Foundation of China (51108230 and 51278241), and the Jiangsu Natural Science Foundation (BK2011016). The authors also thank Vanilla Chen from Biolin Scientific Co., Ltd. in the Shanghai representative office and Prof. Dongqiang Zhu from Nanjing University for their kind help on the QCM-D experiments.

REFERENCES

(1) Barwal, A.; Chaudhary, R. To Study the Performance of Biocarriers in Moving Bed Biofilm Reactor (MBBR) Technology and Kinetics of Biofilm for Retrofitting the Existing Aerobic Treatment Systems: a Review. *Rev. Environ. Sci. Bio/Technol.* **2014**, *13*, 285−299.

(2) Persson, F.; Sultana, R.; Suarez, M.; Hermansson, M.; Plaza, E.; Wilén, B. M. Structure and Composition of Biofilm Communities in a Moving Bed Biofilm Reactor for Nitritation-Anammox at Low Temperatures. *Bioresour. Technol.* **2014**, *154*, 267−273.

(3) Gilbert, E. M.; Agrawal, S.; Karst, S. M.; Horn, H.; Nielsen, P. H.; Lackner, S. Low Temperature Partial Nitritation/Anammox in a Moving Bed Biofilm Reactor Treating Low Strength Wastewater. *Environ. Sci. Technol.* **2014**, *48*, 8784−8792.

(4) Peng, X.; Guo, F.; Ju, F.; Zhang, T. Shifts in the Microbial Community, Nitrifiers and Denitrifiers in the Biofilm in a Full-scale Rotating Biological Contactor. *Environ. Sci. Technol.* **2014**, *48*, 8044−8052.

(5) Simões, M.; Simões, L. C.; Vieira, M. J. A Review of Current and Emergent Biofilm Control Strategies. *LWT – Food Sci. Technol.* **2010**, *43*, 573−583.

(6) O'Toole, G.; Kaplan, H. B.; Kolter, R. Biofilm Formation as Microbial Development. *Annu. Rev. Microbiol.* **2000**, *54*, 49−79.

(7) Verstraeten, N.; Braeken, K.; Debkumari, B.; Fauvart, M.; Fransaer, J.; Vermant, J.; Michiels, J. Living on a Surface: Swarming and Biofilm Formation. *Trends Microbiol.* **2008**, *16*, 496−506.

(8) Paul, E.; Ochoa, J. C.; Pechaud, Y.; Liu, Y.; Line, A. Effect of Shear Stress and Growth Conditions on Detachment and Physical Properties of Biofilms. *Water Res.* **2012**, *46*, 5499−5508.

(9) Tang, L.; Pillai, S.; Revsbech, N. P.; Schramm, A.; Bischoff, C.; Meyer, R. L. Biofilm Retention on Surfaces with Variable Roughness and Hydrophobicity. *Biofouling* **2011**, *27*, 111−121.

(10) Bryers, J. D.; Ratner, B. D. Bioinspired Implant Materials Befuddle Bacteria. *Mater. Today* **2004**, *70*, 232−237.

DOI: 10.1021/acsami.5b00324
ACS Appl. Mater. Interfaces 2015, 7, 7222−7230

(11) Hall-Stoodley, L.; Stoodley, P. Developmental Regulation of Microbial Biofilms. *Curr. Opin. Biotechnol.* **2002**, *13*, 228−233.
(12) Li, Y.; Su, Y.; Zhao, X.; He, X.; Zhang, R.; Zhao, J.; Fan, X.; Jiang, Z. Antifouling, High-flux Nanofiltration Membranes Enabled by Dual Functional Polydopamine. *ACS Appl. Mater. Interfaces* **2014**, *6*, 5548−57.
(13) Su, X.; Tian, Y.; Zuo, W.; Zhang, J.; Li, H.; Pan, X. Static Adsorptive Fouling of Extracellular Polymeric Substances with Different Membrane Materials. *Water Res.* **2014**, *50*, 267−277.
(14) Bernstein, R.; Freger, V.; Lee, J. H.; Kim, Y. G.; Lee, J.; Herzberg, M. 'Should I Stay or Should I Go?' Bacterial Attachment vs Biofilm Formation on Surface-Modified Membranes. *Biofouling* **2014**, *30*, 367−376.
(15) Zhang, Y. Z.; Du, B. Y.; Chen, X. N.; Ma, H. W. Convergence of Dissipation and Impedance Analysis of Quartz Crystal Microbalance Studies. *Anal. Chem.* **2009**, *81*, 642−648.
(16) Herzberg, M.; Sweity, A.; Brami, M.; Kaufman, Y.; Freger, V.; Oron, G.; Belfer, S.; Kasher, R. Surface Properties and Reduced Biofouling of Graft-Copolymers That Possess Oppositely Charged Groups. *Biomacromolecules* **2011**, *12*, 1169−1177.
(17) Sweity, A.; Ying, W.; Ali-Shtaye, M. S.; Yang, F.; Bick, A.; Oron, G.; Herzberg, M. Relation between EPS Adherence, Viscoelastic Properties, and MBR Operation: Biofouling Study with QCM-D. *Water Res.* **2011**, *45*, 6430−6440.
(18) Herzberg, M.; Kang, S.; Elimelech, M. Role of Extracellular Polymeric Substances (EPS) in Biofouling of Reverse Osmosis Membranes. *Environ. Sci. Technol.* **2009**, *43*, 4393−4398.
(19) Wu, J.; Contreras, A. E.; Li, Q. Studying the Impact of RO Membrane Surface Functional Groups on Alginate Fouling in Seawater Desalination. *J. Membr. Sci.* **2014**, *458*, 120−127.
(20) Sweity, A.; Ying, W.; Belfer, S.; Oron, G.; Herzberg, M. pH Effects on the Adherence and Fouling Propensity of Extracellular Polymeric Substances in a Membrane Bioreactor. *J. Membr. Sci.* **2011**, *378*, 186−193.
(21) Orgad, O.; Oren, Y.; Walker, S. L.; Herzberg, M. The Role of Alginate in *Pseudomonas aeruginosa* EPS Adherence, Viscoelastic Properties and Cell Attachment. *Biofouling* **2011**, *27*, 787−798.
(22) Zhu, P. T.; Long, G. Y.; Ni, J. R.; Tong, M. P. Deposition Kinetics of Extracellular Polymeric Substances (EPS) on Silica in Monovalent and Divalent Salts. *Environ. Sci. Technol.* **2009**, *43*, 5699−5704.
(23) Long, G. Y.; Zhu, P. T.; Shen, Y.; Tong, M. P. Influence of Extracellular Polymeric Substances (EPS) on Deposition Kinetics of Bacteria. *Environ. Sci. Technol.* **2009**, *43*, 2308−2314.
(24) Manabe, K.; Nishizawa, S.; Shiratori, S. Porous Surface Structure Fabricated by Breath Figures that Suppresses *Pseudomonas aeruginosa* Biofilm Formation. *ACS Appl. Mater. Interfaces* **2013**, *5*, 11900−11905.
(25) Ying, W.; Yang, F.; Bick, A.; Oron, G.; Herzberg, M. Extracellular Polymeric Substances (EPS) in a Hybrid Growth Membrane Bioreactor (HG-MBR): Viscoelastic and Adherence Characteristics. *Environ. Sci. Technol.* **2010**, *44*, 8636−8643.
(26) Giasson, S.; Lagleize, J. M.; Rodriguez-Hernandez, J.; Drummond, C. Boundary Lubricant Polymer Films: Effect of Cross-linking. *Langmuir* **2013**, *29*, 12936−12949.
(27) Armanious, A.; Aeppli, M.; Sander, M. Dissolved Organic Matter Adsorption to Model Surfaces: Adlayer Formation, Properties, and Dynamics at the Nanoscale. *Environ. Sci. Technol.* **2014**, *48*, 9420−9429.
(28) Myint, A. A.; Lee, W.; Mun, S.; Ahn, C. H.; Lee, S.; Yoon, J. Influence of Membrane Surface Properties on the Behavior of Initial Bacterial Adhesion and Biofilm Development onto Nanofiltration Membranes. *Biofouling* **2010**, *26*, 313−321.
(29) Jiang, J.; Zhu, L.; Zhu, L.; Zhang, H.; Zhu, B.; Xu, Y. Antifouling and Antimicrobial Polymer Membranes Based on Bioinspired Polydopamine and Strong Hydrogen-Bonded Poly(*N*-vinyl pyrrolidone). *ACS Appl. Mater. Interfaces* **2013**, *5*, 12895−12904.
(30) Liu, C. Z.; Meenan, B. J. Effect of Air Plasma Processing on the Adsorption Behaviour of Bovine Serum Albumin on Spin-Coated PMMA Surfaces. *Journal of Bionic Engineering* **2008**, *5*, 204−214.
(31) Wang, Z. W.; Mei, X. J.; Ma, J. X.; Grasmick, A.; Wu, Z. C. Potential Foulants and Fouling Indicators in MBRs: A Critical Review. *Sep. Sci. Technol.* **2013**, *48*, 22−50.
(32) *Standard Methods for the Examination of Water and Wastewater*; American Public Health Association: WA, 1998.
(33) Bradford, M. M. A Rapid and Sensitive Method for the Quantitation of Microgram Quantities of Protein Utilizing the Principle of Protein-Dye Binding. *Anal. Biochem.* **1976**, *72*, 248−254.
(34) DuBois, M.; Gilles, K. A.; Hamilton, J. K.; Rebers, P. A.; Smith, F. Colorimetric Method for Determination of Sugars and Related Substances. *Anal. Chem.* **1956**, *28*, 350−356.
(35) Frølund, B.; Griebe, T.; Nielsen, P. H. Enzymatic Activity in the Activated-Sludge Floc Matrix. *Appl. Microbiol. Biotechnol.* **1995**, *43*, 755−761.
(36) Huang, H.; Ren, H. Q.; Ding, L. L.; Geng, J. J.; Xu, K.; Zhang, Y. Aging Biofilm from a Full-Scale Moving Bed Biofilm Reactor: Characterization and Enzymatic Treatment Study. *Bioresour. Technol.* **2014**, *154*, 122−130.
(37) Wang, T.; Wang, X. W.; Long, Y. C.; Liu, G. M.; Zhang, G. Z. Ion-Specific Conformational Behavior of Polyzwitterionic Brushes: Exploiting It for Protein Adsorption/Desorption Control. *Langmuir* **2013**, *29*, 6588−6596.
(38) Voinova, M. V.; Rodahl, M.; Jonson, M.; Kasemo, B. Viscoelastic Acoustic Response of Layered Polymer Films at Fluid-Solid Interfaces: Continuum Mechanics Approach. *Phys. Scr.* **1999**, *59*, 391−396.
(39) Yi, P.; Chen, K. L. Release Kinetics of Multiwalled Carbon Nanotubes Deposited on Silica Surfaces: QCM-D Measurements and Modeling. *Environ. Sci. Technol.* **2014**, *48*, 4406−4413.
(40) Yi, P.; Chen, K. L. Influence of Solution Chemistry on the Release of Multiwalled Carbon Nanotubes from Silica Surfaces. *Environ. Sci. Technol.* **2013**, *47*, 12211−12218.
(41) Olsson, A. L. J.; van der Mei, H. C.; Johannsmann, D.; Busscher, H. J.; Sharma, P. K. Probing Colloid-Substratum Contact Stiffness by Acoustic Sensing in a Liquid Phase. *Anal. Chem.* **2012**, *84*, 4504−4512.
(42) Orski, S. V.; Kundu, S.; Gross, R.; Beers, K. L. Design and Implementation of Two-Dimensional Polymer Adsorption Models: Evaluating the Stability of *Candida antarctica* Lipase B/Solid-Support Interfaces by QCM-D. *Biomacromolecules* **2013**, *14*, 377−386.
(43) Xiao, K.; Shen, Y. X.; Liang, S.; Liang, P.; Wang, X. M.; Huang, X. A Systematic Analysis of Fouling Evolution and Irreversibility Behaviors of MBR Supernatant Hydrophilic/Hydrophobic Fractions during Microfiltration. *J. Membr. Sci.* **2014**, *467*, 206−216.
(44) Li, H. S.; Wen, Y.; Cao, A. S.; Huang, J. S.; Zhou, Q.; Somasundaran, P. The Influence of Additives (Ca^{2+}, Al^{3+}, and Fe^{3+}) on the Interaction Energy and Loosely Bound Extracellular Polymeric Substances (EPS) of Activated Sludge and Their Flocculation Mechanisms. *Bioresour. Technol.* **2012**, *114*, 188−194.
(45) Listiarini, K.; Chun, W.; Sun, D. D.; Leckie, J. O. Fouling Mechanism and Resistance Analyses of Systems Containing Sodium Alginate, Calcium, Alum and Their Combination in Dead-End Fouling of Nanofiltration Membranes. *J. Membr. Sci.* **2009**, *344*, 244−251.
(46) Wang, Q. Y.; Wang, Z. W.; Zhu, C. W.; Mei, X. J.; Wu, Z. C. Assessment of SMP Fouling by Foulant-Membrane Interaction Energy Analysis. *J. Membr. Sci.* **2013**, *446*, 154−163.
(47) Lin, T.; Lu, Z.; Chen, W. Interaction Mechanisms and Predictions on Membrane Fouling in an Ultrafiltration System, Using the XDLVO Approach. *J. Membr. Sci.* **2014**, *461*, 49−58.
(48) Zhang, P.; Chen, Y. P.; Guo, J. S.; Shen, Y.; Yang, J. X.; Fang, F.; Li, C.; Gao, X.; Wang, G. X. Adsorption Behavior of Tightly Bound Extracellular Polymeric Substances on Model Organic Surfaces under Different pH and Cations with Surface Plasmon Resonance. *Water Res.* **2014**, *57*, 31−39.
(49) Chen, W.; Westerhoff, P.; Leenheer, J. A.; Booksh, K. Fluorescence Excitation-Emission Matrix Regional Integration to Quantify Spectra for Dissolved Organic Matter. *Environ. Sci. Technol.* **2003**, *37*, 5701−5710.
(50) Liu, T.; Chen, Z. L.; Yu, W. Z.; You, S. J. Characterization of Organic Membrane Foulants in a Submerged Membrane Bioreactor

DOI: 10.1021/acsami.5b00324
ACS Appl. Mater. Interfaces 2015, 7, 7222−7230

with Pre-ozonation Using Three-Dimensional Excitation-Emission Matrix Fluorescence Spectroscopy. *Water Res.* **2011**, *45*, 2111−2121.
(51) Yang, W. L.; Li, X. C.; Pan, B. C.; Lv, L.; Zhang, W. M. Effective Removal of Effluent Organic Matter (EfOM) from Bio-Treated Coking Wastewater by a Recyclable Aminated Hyper-Cross-Linked Polymer. *Water Res.* **2013**, *47*, 4730−4738.
(52) Schofield, A. L.; Rudd, T. R.; Martin, D. S.; Fernig, D. G.; Edwards, C. Real-Time Monitoring of the Development and Stability of Biofilms of *Streptococcus mutans* Using the Quartz Crystal Microbalance with Dissipation Monitoring. *Biosens. Bioelectron.* **2007**, *23*, 407−413.
(53) Tsuneda, S.; Aikawa, H.; Hayashi, H.; Yuasa, A.; Hirata, A. Extracellular Polymeric Substances Responsible for Bacterial Adhesion onto Solid Surface. *FEMS Microbiol. Lett.* **2003**, *223*, 287−292.
(54) Ganesan, M.; Stewart, E. J.; Szafranski, J.; Satorius, A. E.; Younger, J. G.; Solomon, M. J. Molar Mass, Entanglement, and Associations of the Biofilm Polysaccharide of *Staphylococcus epidermidis*. *Biomacromolecules* **2013**, *14*, 1474−1481.
(55) Chen, L.; Tian, Y.; Cao, C. Q.; Zhang, J.; Li, Z. N. Interaction Energy Evaluation of Soluble Microbial Products (SMP) on Different Membrane Surfaces: Role of the Reconstructed Membrane Topology. *Water Res.* **2012**, *46*, 2693−2704.

DOI: 10.1021/acsami.5b00324
ACS Appl. Mater. Interfaces 2015, 7, 7222−7230